https://doi.org/10.3311/PPci.21798
Creative Commons Attribution 

Periodica Polytechnica Civil Engineering, 67(4), pp. 1001–1015, 2023

# Effects of Different Wall Openings on the Cyclic Behavior of Aerated Concrete Block Infilled RC Frames

Batuhan Aykanat[1*], Mehmet Emin Arslan[1], Anıl Şen[1]

[1] Düzce University, Engineering Faculty, Department of Civil Engineering, 81620 Düzce, Türkiye
[*] Corresponding author, e-mail: batuhanaykanat@duzce.edu.tr

Received: 04 January 2023, Accepted: 25 May 2023, Published online: 14 June 2023

**Abstract**

In the current study, the effects of infilled reinforced concrete (RC) frames with different window and door openings under cyclic loads were investigated. For this purpose, five in-filled RC frames with different infill wall openings were produced. The main parameters to evaluate overall performance of the RC frames with infill walls, the load carrying capacities, displacement ductility, stiffness degradation and energy dissipation capacities were determined using obtained results. At the end of the study, even if the opening ratios are the equal, it has been observed that the location and number of openings have a significant effect on the behavior and failure pattern of the RC frames. Also, increase in the openings ratio decreases the load carrying capacity, and energy consumption capacity. Based on these results, it is suggested that infill walls affect the structural behavior and failure pattern. Therefore, infill wall openings should be considered in the design of RC structures.

**Keywords**

RC frame, infill wall openings, aerated concrete, cyclic loading, experimental study

## 1 Introduction

Infill walls are often neglected and treated as non-structural elements due to their low load carrying capacity [1]. Although such an assumption makes it easy to design, and evaluate structures, it can lead to uncertainty in structural behavior and undesirable consequences [2]. Infill walls, which are generally considered as dead loads, affect the load carrying capacity, stiffness, and energy dissipation of RC frames. Studies after the damage of the earthquakes show that infill walls have changed the seismic behavior of the structure and cause different failure modes to the buildings [3]. When the infill walls are constructed adjacent to the frame members, they tend to separate from the frame member under the diagonal compression. With the increasing seismic effects, on the walls cracks occur at the weak points, crushes and collapses can be observed [4–8]. In addition to all these, the door and window openings needed for ventilation and lighting requirements should also be considered in walls and frames behavior. Although infill walls significantly affect the structural behavior of frames, in the structural design the interaction of infill walls and frames is generally neglected [9–13]. Therefore, in recent years, many researchers have focused on investigating the behavior of in-filled frame systems in regions with high seismic activity [14].

Cheng et al. [14], in their study, investigated the mechanical properties of the steel frame with infill walls. Shan et al. [15], investigated the effects of partial infill walls on the failure behavior of RC frame systems. De Angelis and Pecce [16], propose a method for describing the out-of-plane structural behavior of infill walls using a simple and cost-effective innovative method based on dynamic tests. Binici et al. [17], investigated the seismic behavior of aerated concrete infill walls and carried out studies to improve their seismic behavior. As a result of their studies, they argued that the methods they proposed are a good alternative for producing earthquake resistant infill walls. Buitrado et al. [18], in order to investigate the effect of infill walls on the strength of RC structures, they carried out their tests on a two-story structure prepared in 1/1 scale. In the tests, based on the scenario of the sudden removal of a column from the system, the contribution of infill walls to the frame performance was examined. Prakash and Satyanarayanan [19], investigated the collapse behavior of a five-story RC structure. They provide an appropriate load transfer and can increase the collapse resistance of RC frames. Jalaeefar and Zargar [20], created 4, 8, and 12 storey models and analyzed these models using the finite element

**Cite this article as:** Aykanat B., Arslan, M. E., Şen A. "Effects of Different Wall Openings on the Cyclic Behavior of Aerated Concrete Block Infilled RC Frames", Periodica Polytechnica Civil Engineering, 67(4), pp. 1001–1015, 2023. https://doi.org/10.3311/PPci.21798

method in order to examine the effects of the earthquake on RC frames with infill walls. Eren et al. [2], evaluated the effects of infill walls on the vertical load bearing capacity of RC frames with a different number of collapse simulations. Bikçe et al. [3], was carried out a study to determine the in-plane behavior of infill walls flexibly joint to RC frames. In the study, RC frames without infill walls and ordinary in-filled RC frames are compared with in-filled RC frames with flexible joints. At the end of the study, it was determined that infill walls with flexible connection points improved in-plane behavior. Furtado et al. [21], investigated the structural behavior of an RC frame with infill walls, an RC frame with infill walls reinforced with Glass Fiber Reinforced Polymer (GFRP), and RC frames with GFRP reinforced infill walls with a window opening in the center. As a result, they found that the window opening in the infill walls reduced the maximum load by 40% and the energy dissipation capacity by approximately 18%.

Also, in recent years, various methods have been proposed to predict the mechanical properties of reinforced concrete frames with infill walls. The results of the studies show that the obtained data and the proposed formulas can be used to predict the mechanical properties of reinforced concrete frames with infill walls [22–24].

In the current study, the structural behavior of RC frames with aerated concrete infill walls with door and window openings of different sizes and locations under cyclic loads were experimentally investigated. By using the findings obtained from the experiments, the load carrying capacities, energy dissipation capacities and failure patterns of the in-filled wall frames were determined.

## 2 Experimental study

### 2.1 Material properties

In the production of the RC frame, ready-mix concrete was used. Mixture proportion of the concrete is given in Table 1. Longitudinal rebar with 12 mm for beam and 14 mm for column were used. Stirrup diameter was 8 mm for both beam and column. Some mechanical properties of rebars and concrete used in the production of RC frames with infill walls are given in Table 1.

In this study, aerated concrete blocks were used as infill wall material. The reason of choosing aerated concrete blocks is that its low cost and widespread using, easy availability and application. Some physical and mechanical properties of aerated concrete blocks are given in the Table 2.

A special mortar was used to bond aerated concrete blocks. Some properties of the adhesive mortar are given in Table 3.

On both sides of the infill walls, 20 mm thick cement-based mill-mixed plaster was applied. Some physical and mechanical properties of mill-mixed plaster are given in the Table 4.

### 2.2 Design of test specimens

Within the scope of the study, five RC frames with infill walls by the dimension of 250 × 225 × 20 cm were produced. The infill wall thickness in reinforced concrete frames is 20 cm. Door and window openings of different sizes have

**Table 2** Some physical and mechanical properties of aerated concrete blocks

| Properties of Aerated Concrete | |
|---|---|
| Dimension (cm) | 60 × 19 × 25 |
| Density (kg/m$^3$) | 400 |
| Compressive Strength (MPa) | 2.5 |
| Thermal Conductivity (W/mK) | 0.13 |

**Table 3** Some properties of adhesive mortar

| Properties of Adhesive Mortar | |
|---|---|
| Workability (min.) | 240 |
| Density (t/m$^3$) | 1.4 ± 1.0 |
| Compressive Strength (MPa) | 5.0 |
| Thermal Conductivity (W/mK) | 0.53 |

**Table 1** Some mechanical properties of rebars and concrete

| | Rebar | | | Concrete | |
|---|---|---|---|---|---|
| | 8 mm | 12 mm | 14 mm | | |
| Yield Strength (N/mm$^2$) | 486.43 | 478.85 | 494.03 | Compressive Strength (N/mm$^2$) | 40.28 |
| Tensile Strength (N/mm$^2$) | 613.88 | 609.76 | 624.21 | Density (kg/m$^3$) | 2.31 |
| Failure Strain (%) | 22.18 | 22.56 | 22.87 | Modulus of Elasticity (MPa) | 39200 |

| Mixture Proportion of Concrete | | | | | | |
|---|---|---|---|---|---|---|
| Aggregate Amounts According to Sieve Pore Openings (kg/m$^3$) | | | | | Amount of Cement (kg/m$^3$) | Water/Cement |
| 0.5–1.0 (mm) | 1.0–2.0 (mm) | 2.0–4.0 (mm) | 4.0–8.0 (mm) | 8.0–16.0 (mm) | | |
| 265.50 | 265.50 | 265.50 | 442.50 | 531.0 | 370 | 0.5 |

**Table 4** Some properties of mill-mixed plaster

| Properties of Mill-Mixed Plaster | |
|---|---|
| Dry Unit Weight (t/m$^3$) | 1.45 ± 1.0 |
| Fresh Unit Weight (t/m$^3$) | 1.8 ± 1.0 |
| Mean Compressive Strength (MPa) | 2.7 |
| Mean Flexural Strength (MPa) | 1.1 |
| Modulus of Elasticity (MPa) | 4750 ± 100 |
| Thermal Conductivity (W/mK) 23.0 °C | 0.420 ± 0.02 |

been left in order to represent the commonly used window and door openings in wall production. The production stages of RC frames with infill walls are shown in Fig. 1.

RCF-1 coded RC frame is the reference test specimen of the study. In the reference specimen, RC frame was fully in-filled with aerated concrete blocks. On both surfaces of the infill walls, 20 mm thick plaster was applied. In order to determine the location of the cracks that will occur during the experiment, the infill wall surfaces were painted with lime. Details of the RCF-1 specimen are shown in Fig. 2.

In the center of the RCF-2 specimen, a 75 × 80 cm window opening was left in order to represent the common appli- cations. During the construction of the infill wall, a lintel of 100 × 15 × 5 cm was placed over the window opening. Concrete and rebars used in the production of


**Fig. 1** Production stages of RC frames with infill walls; (a) Preparation of foundation, (b) Preparation of rebars, (c) Preparation of mold, (d) Pouring of concrete, (e) Producing of infill wall, (f) Plastering the wall surface, (g) Dimensions and reinforcement details of the test frames

RC frames were also used in the production of lintels. The plaster thickness applied to the wall surface was 20 mm. Details of the RCF-2 specimen are shown in Fig. 3.

In the center of the RCF-3 specimen, 2 windows openings of the same dimensions (50 × 60 cm) were left. The aim here is to determine the effect of leaving the opening area equal to the RCF-2 specimen in a different position on the wall behavior. As in all other frames, 80 × 15 × 5 cm lintels are used in the places that come over the openings. Also, 20 mm plaster was applied to the infill wall as well. Details of the RCF-3 specimen are shown in Fig. 4.

RCF-4 specimen was produced to represent the infill walls with door openings used today. A 50 × 120 cm door opening was left on the infill wall. A 70 × 15 × 5 cm lintel is placed over the door opening. Plaster with 20 mm thickness was applied to the infill wall. Details of the RCF-4 specimen are shown in Fig. 5.

In the RCF-5 specimen, a door opening (50 × 120 cm) and a window opening (60 × 50 cm) were left. A lintel is placed over the door and window openings. Also 20 mm plaster was applied to the infill wall, and it was painted with lime. Details of the RCF-5 specimen are shown in Fig. 6.

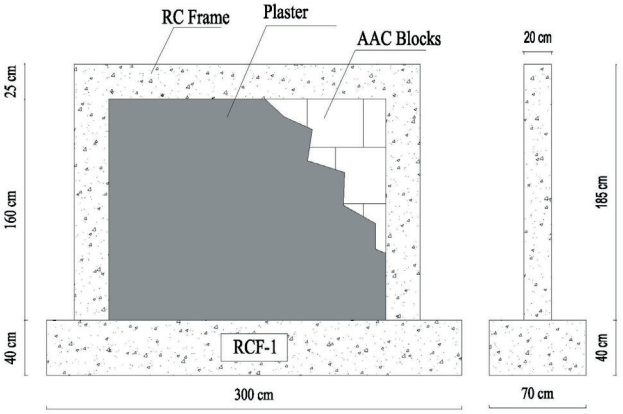


**Fig. 2** Dimension and materials details of RCF-1 specimen

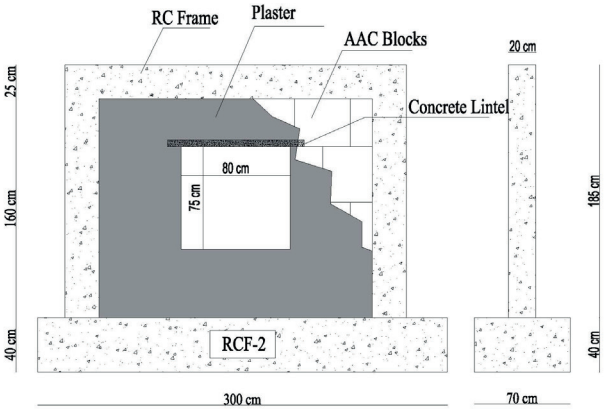


**Fig. 3** Dimension and materials details of RCF-2 specimen

### 2.3 Test setup and procedure

The main purpose of the study is to comparatively examine the effects of the infill wall openings and locations on the RC frame behaviors under cyclic loading. For this purpose, the structural behavior of RC frames with infill walls under cyclic loads has been comparatively investigated. By using the hysteretic load-displacement curves obtained at the end of the tests, the load carrying capacities, energy dissipation capacities and crack formations of the test specimen have been determined.

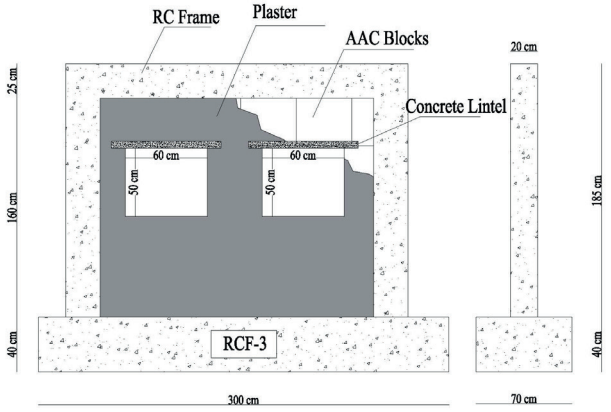


**Fig. 4** Dimension and materials details of RCF-3specimen

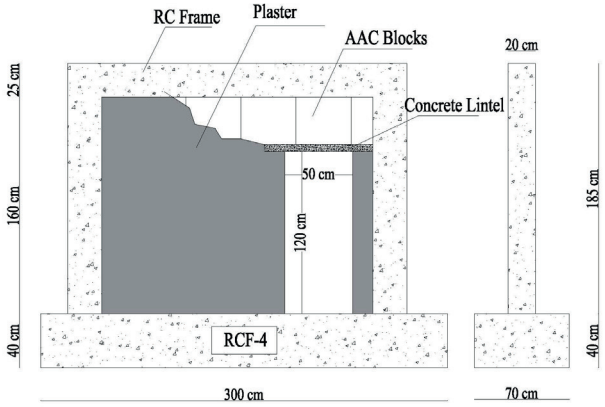


**Fig. 5** Dimension and materials details of RCF-4 specimen

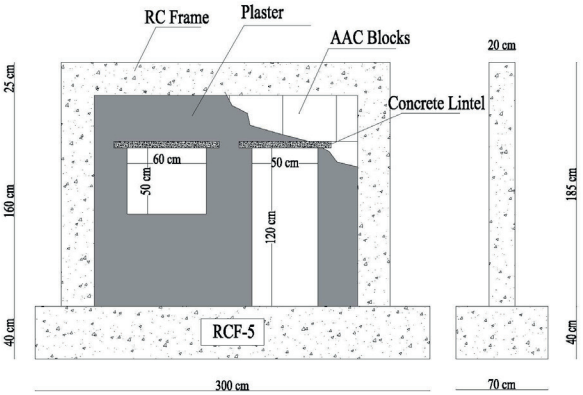


**Fig. 6** Dimension and materials details of RCF-5 specimen

Horizontal cyclic load was applied to all of the frames with the help of a servo-hydraulic actuator. The loading protocol recommended by FEMA 461 [25] was used in the tests. The applied displacements consist of cycles corresponding to drift ratios of 0.15%, 0.20%, 0.25%, 0.35%, 0.50%, 0.75%, 1.00%, 1.40%, 1.75%, 2.20%, 2.75%, 3.50%, 4.00%, 4.50%, 5.00%, 5.50%, 6.00%, 6.50%. The reason for using drift ratios higher than the 3.5% drift ratio is to see the complete failure of the walls. The displacement cycle was repeated twice for each drift ratio. The loading protocol is shown in Fig. 7.

Loads were measured with a 500 kN capacity load cell in the test setup used to apply cyclic loads to the test specimens. Displacements corresponding to the load were measured with an LVDT with a measuring capacity of 500 mm placed in the activator. Also, peak point displacements additionally were measured by the help of 300 mm linear potentiometric displacement transducer (LPDT). All data were recorded to the computer at 0.125 sec intervals. Details of the experimental setup are shown in Fig. 8.

## 3 Experimental results

The hysteretic load-displacement curves of RC frames with infill walls are presented in Fig. 9. When the cyclic load-displacement curves are examined, displacements for each cycle are the same. This proves that loading protocol was applied properly to the frames in the pushing (-) and pulling (+) directions.

## 4 Discussion

In this section, the maximum load obtained from the cyclic loading of RC frames with infill wall and the corresponding displacement values are examined. The backbone curves of the 1st and 2nd cycles obtained with these values are given below. In addition, F/Fmax curves obtained by dividing each load value in the 1st and 2nd cycles by the maximum load are also given below. The level of damage on the wall and its level in the progressive loading steps were discussed.

### 4.1 Load carrying capacities

#### 4.1.1 RCF-1

When the Fig. 10(a) is examined, it is seen that the RCF1 frame behaves symmetrically. The maximum load and the corresponding displacements were determined as 190.41 kN and 30.108 mm in the pulling direction (+) and 210.45 kN and 24.074 mm in the pushing direction (-), respectively. When the second cycle of loading is examined, values of 174.251 kN and 20.078 mm in the pulling direction (+) and 190.54 kN and 24.074 mm in the pushing direction (-) were reached. According to the F/Fmax curve (Fig. 10(b)), the maximum load values decreased by approximately 8.5% in the pulling direction and approximately 9.5% in the pushing direction between two cycles. The drift ratio, in which these values started to increase rapidly, was determined as approximately 1.7%.

The ultimate decrease in load was found at a drift ratio of about 3.5%. At a 3.5% drift ratio, the load difference between the two cycles reached approximately 22%, and since this ratio is greater than 15% according to the literature, it can be accepted that the wall has lost its carrying capacity [26–29].

#### 4.1.2 RCF-2

When the backbone curve in Fig. 11(a) is examined, it is seen that the RCF-2 frame reaches a maximum load of 165.57 kN and a displacement of 30.10 mm in the pulling direction. In the pushing direction, it reached a maximum load of 183 kN and a displacement of 24.07 mm. According to the *F*/*Fmax* curve (Fig. 11(b)), it is seen that the load

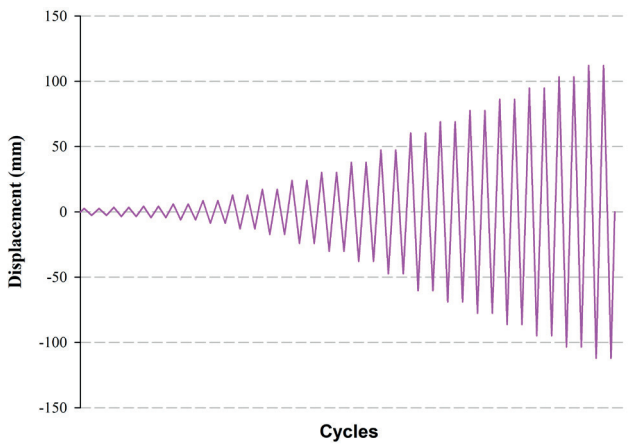


**Fig. 7** Reverse cyclic lateral loading protocol

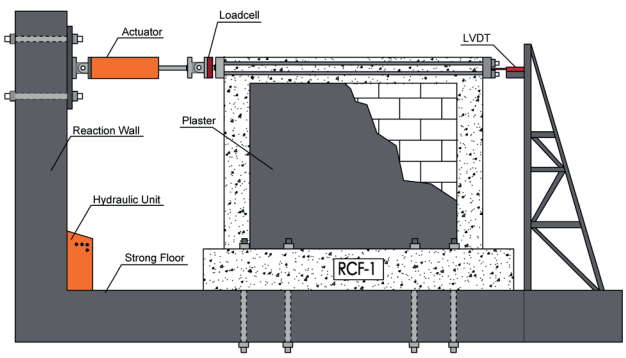


**Fig. 8** Test setup

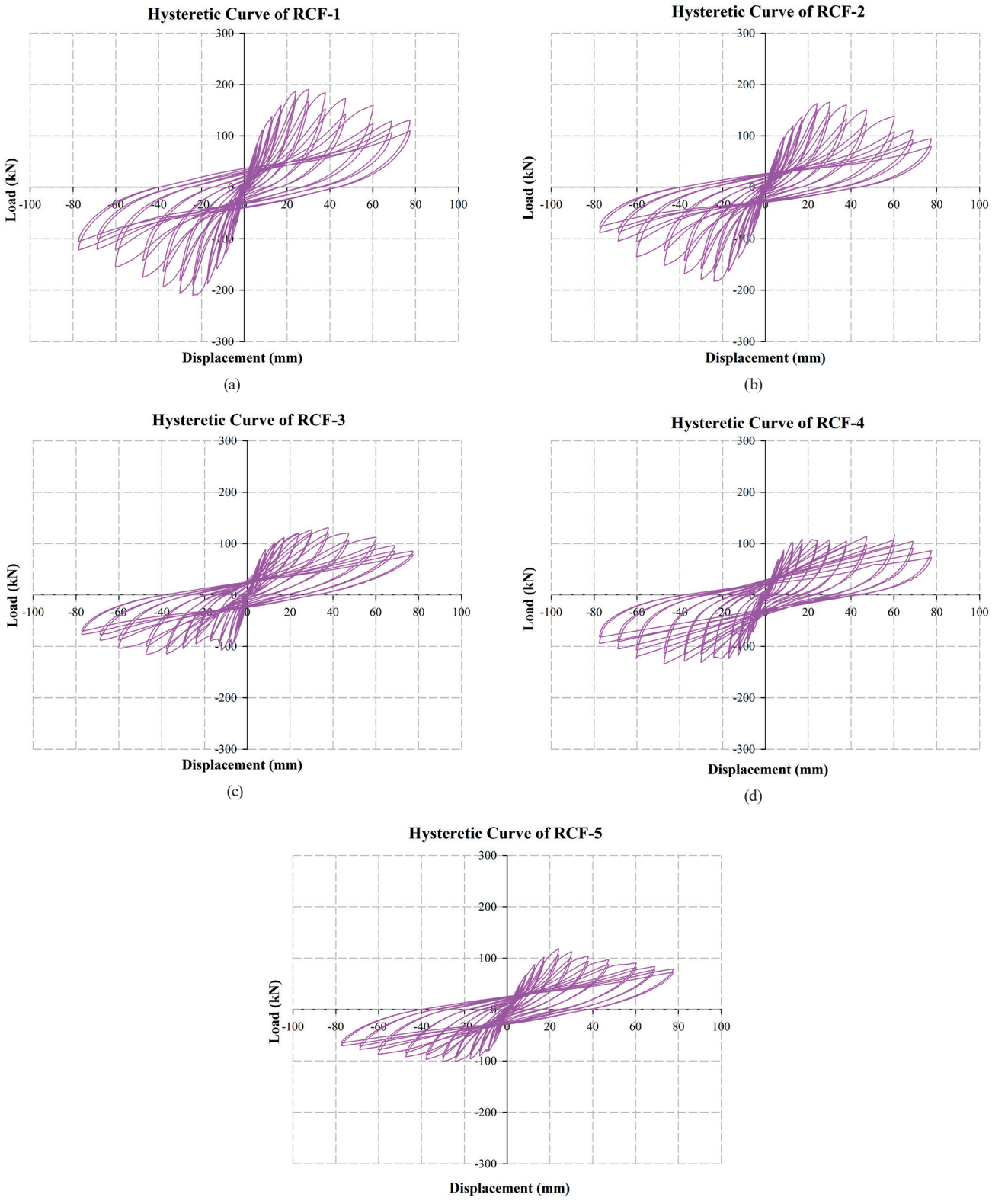


**Fig. 9** Hysteretic load-displacement curves of reinforces concrete frames, Hyteretic curve of (a) RCF-1, (b) RCF-2, (c) RCF-3, (d) RCF-4, (e) RCF-5

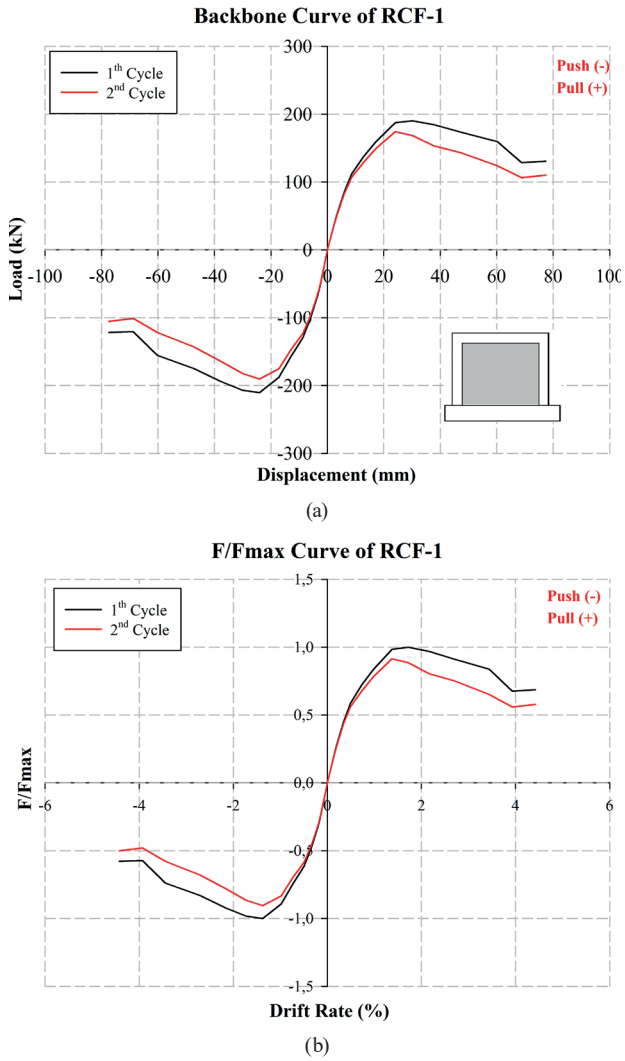


**Fig. 10** (a) Backbone curve of RCF-1, (b) F/Fmax Curve of RCF-1

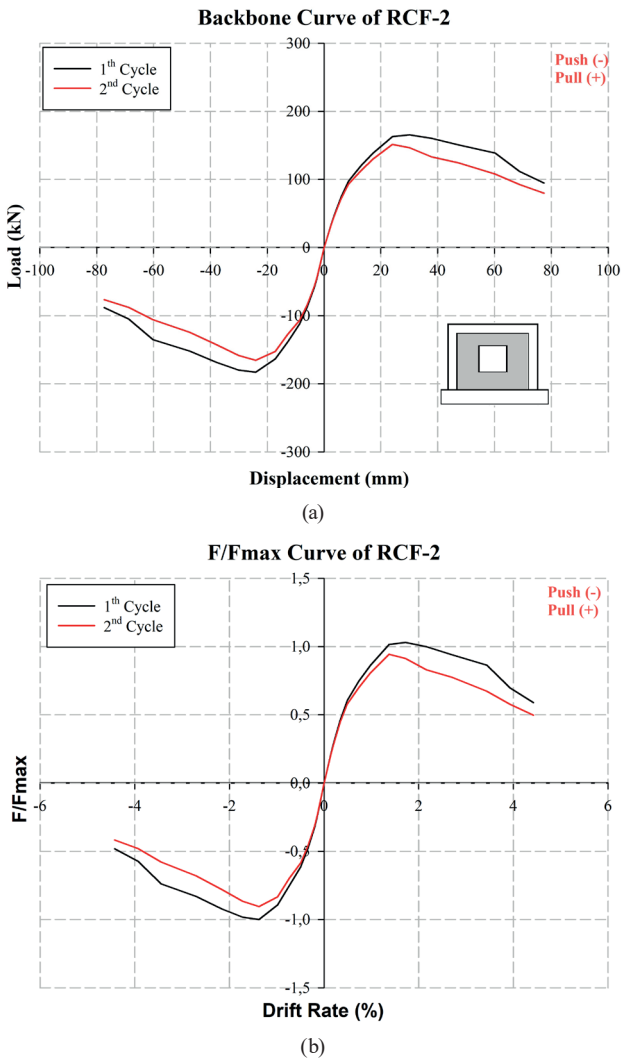


**Fig. 11** (a) Backbone curve of RCF-2, (b) F/Fmax Curve of RCF-2

carrying capacity between the two cycles is approximately 8% lower in the pulling direction and approximately 9.4% in the pushing direction. When the decreases in the load according to the drift ratio are examined, the ultimate decrease was observed in the 12th cycle at the 3.5% drift ratio in both directions. The load carrying capacity of the RCF-2 frame was decreased by approximately 13% in the pulling and pushing direction compared to the RCF-1 frame. It has been determined that the window openings left in the infill wall decrease the load carrying capacity.

### 4.1.3 RCF-3

When the backbone curve of the RCF-3 frame was examined (Fig. 12(a)), a maximum load of 130 kN and a displacement of 37.74 mm was reached in the pulling direction. In the pushing direction, a maximum load of 116.34 kN and a displacement of 47.16 mm was reached. In the second cycle of loading, the maximum load decreased by approximately 8% in the pulling direction and approximately 10% in the pushing direction (Fig. 12(b)). Compared to the RCF-1, the load bearing capacity of the RCF-3 frame decreased by approximately 32% in the pulling direction and 45% in the pushing direction. The decrease in load carrying capacity is 32% greater than with the RCF-2 frame. This reveals that the opening position significantly changes the load carrying capacity.

### 4.1.4 RCF-4

According to the backbone curve (Fig. 13(a)), the RCF-4 frame have been reached a maximum load of 117.01 kN and a displacement of 60.33 mm in the pulling direction. When the pushing direction is examined, a maximum load of 131.28 kN and a corresponding displacement of 30.16 mm have been reached. When the F/Fmax curve is examined (Fig. 13(b)), the maximum loads decreased by 15.4% in the pulling direction and 13% in the pushing

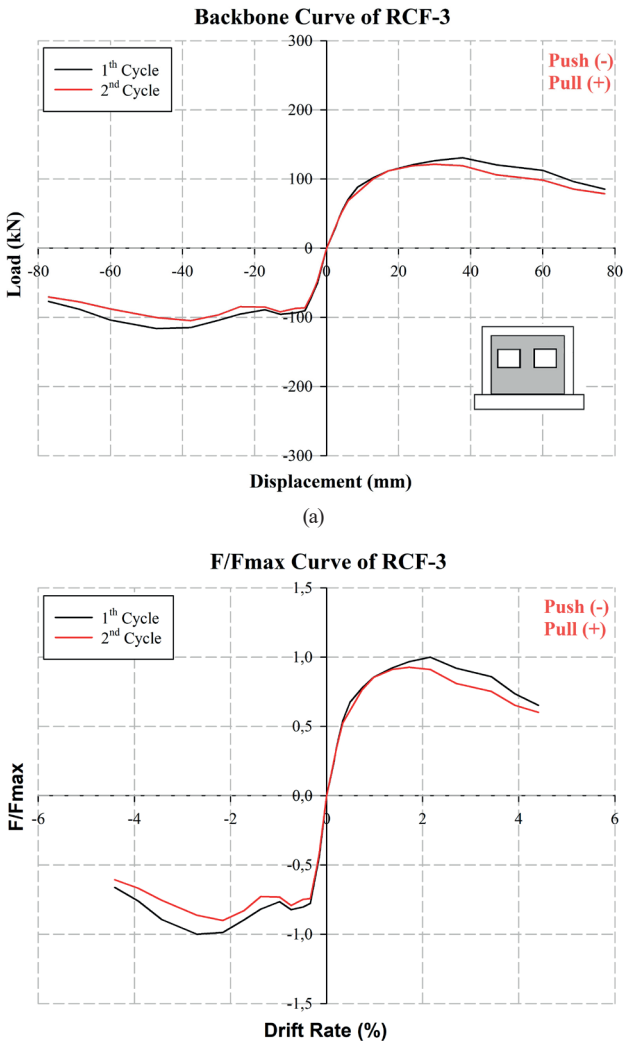


**Fig. 12** (a) Backbone curve of RCF-3, (b) F/Fmax Curve of RCF-3

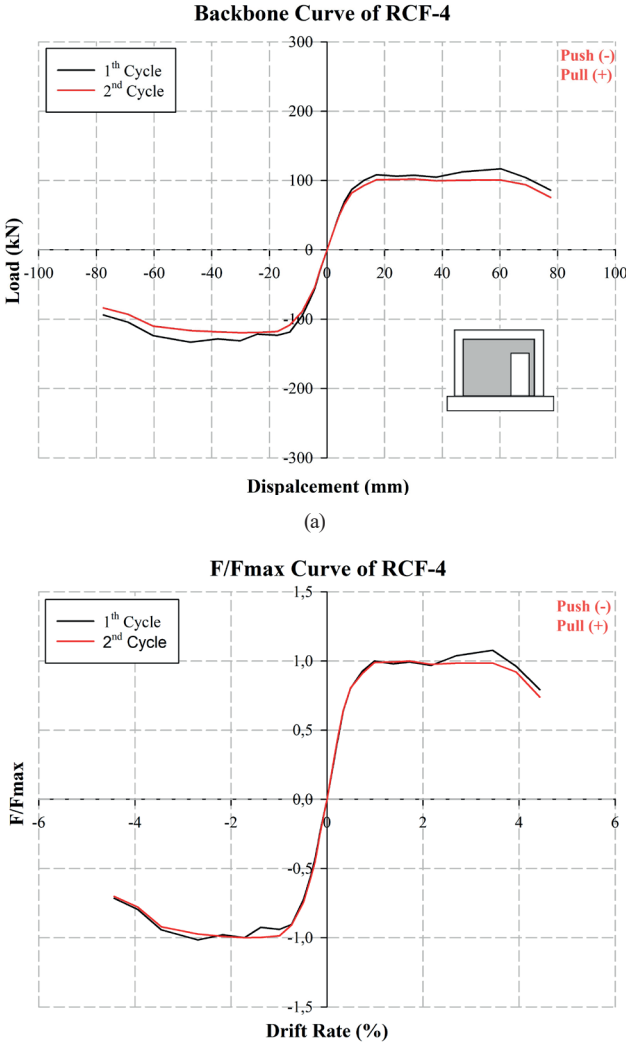


**Fig. 13** (a) Backbone curve of RCF-4, (b) F/Fmax Curve of RCF-4

direction in the second cycle. Compared to the reference, the load carrying capacity decreased by 38.4% in the pulling direction and 38% in the pushing direction. It has been determined that the positions of the openings left in the infill walls change the load carrying capacity. According to these results, it is seen that the RCF-4 frame has a similar load carrying capacity with the RCF-3.

#### 4.1.5 RCF-5

When Fig. 14(a) is examined, the RCF-5 frame has reached a maximum load of 118.46 kN and a displacement of 24.14 mm in the pulling direction, and a maximum load of 101.7 kN and a displacement of 30.16 mm in the pushing direction. In the second cycle of loading, the maximum loads decreased by 10% in the pulling direction and 7% in the pushing direction (Fig. 14(b)). The ultimate decrease in load was found at a drift ratio of about 1.38%. Compared to the RCF-1, it was determined that the load carrying capacity decreased by 38% in the pulling direction and 52% in the pushing direction. The RCF-5 frame, which has the most opening area compared to the other frames, reached the lowest load carrying capacity (Fig. 15 and Fig. 16).

### 4.2 Energy dissipation capacities

The total dissipated energies of the test specimens were obtained by cumulative summing of the areas under the load-displacement curve for each cycle (Fig. 17). The total dissipated energies of the specimens are given in Fig. 18 and also the cumulative total dissipated energies are given in Fig. 19 comparatively.

When Fig. 18 and Fig. 19 are examined, it is seen that the openings left in the infill walls decrease the energy dissipation capacity. The RCF-1 specimen showed the best performance in terms of total energy dissipation. When

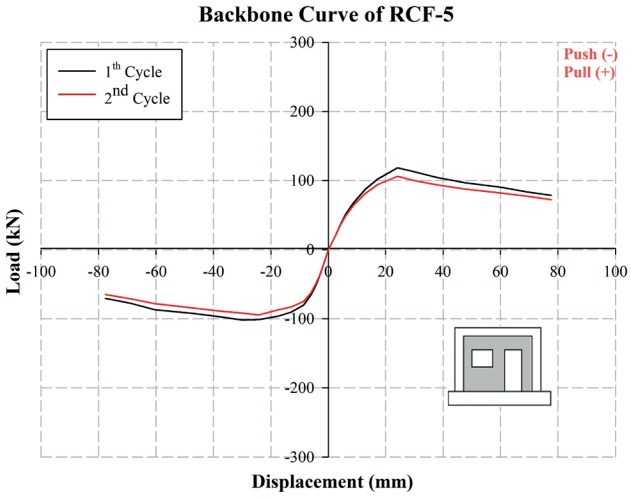


(a)

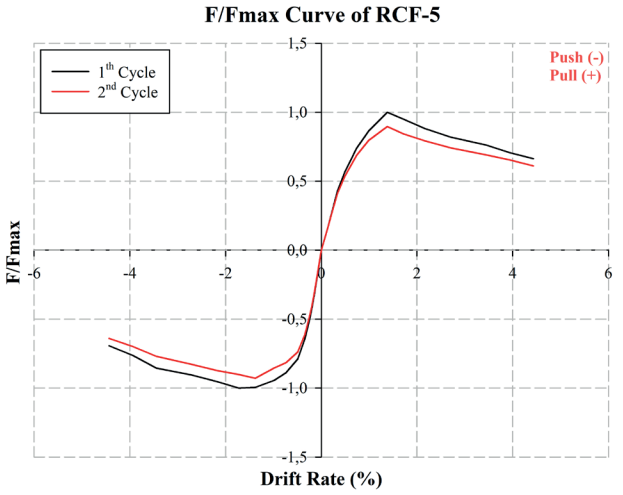


(b)

**Fig. 14** (a) Backbone curve of RCF-5, (b) F/Fmax Curve of RCF-5

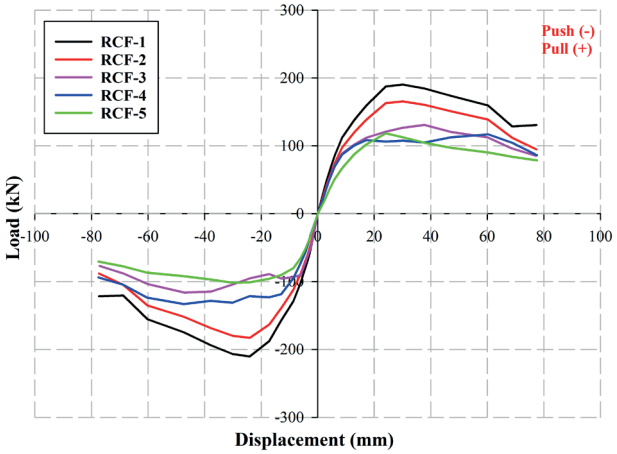


**Fig. 15** Comparative backbone curves

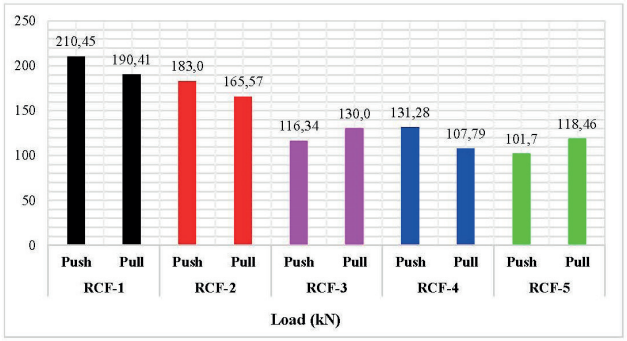


**Fig. 16** Comparative maximum load

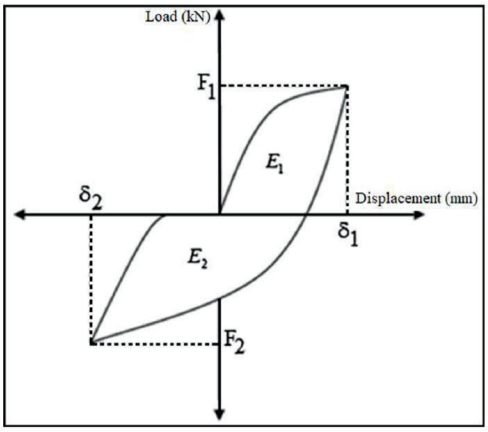


**Fig. 17** Calculation of dissipated energies for each cycle

the total amount of dissipated energy is compared with the RCF-1, a decrease of 13%, 33.5%, 31.9% and 42.3% was observed in the other specimens, respectively. Although the opening ratios in the RCF-2, RCF-3 and RCF-4 samples were equal, the difference in the opening positions changed their energy dissipation capacity.

### 4.3 Stiffness degradations

The stiffness degradations of the specimens were calculated according to Fig. 20 with the help of the slopes of the curves drawn from the peak loads for each cycle in the tensile and repulsive directions. The stiffness degradation is important for interpreting the behavior of specimens. In determining the behaviors, a certain drift ratio should be determined in order to ignore the effect of local damages that may occur at the beginning of the test and can be misleading. It is thought that the evaluations made in this way will give more reliable results. The drift ratios and stiffness degradation values are given in Fig. 21. The load capacities and stiffness of in-filled RC frames at different drift ratios are given Table 5.

The order from highest to lowest in initial stiffness and stiffness degradation is from RCF-1 to RCF-5, as in load carrying and energy dissipation capacities.

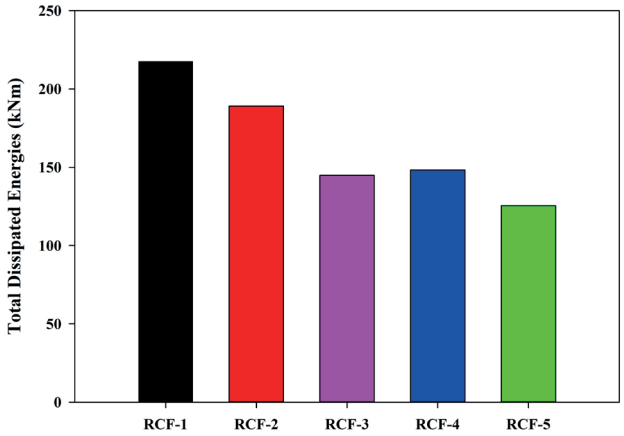


**Fig. 18** Total dissipated energies of the test specimens

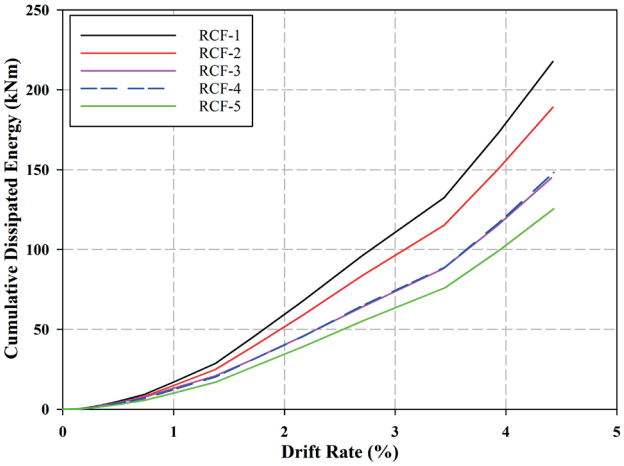


**Fig. 19** Cumulative dissipated energies of the test specimens

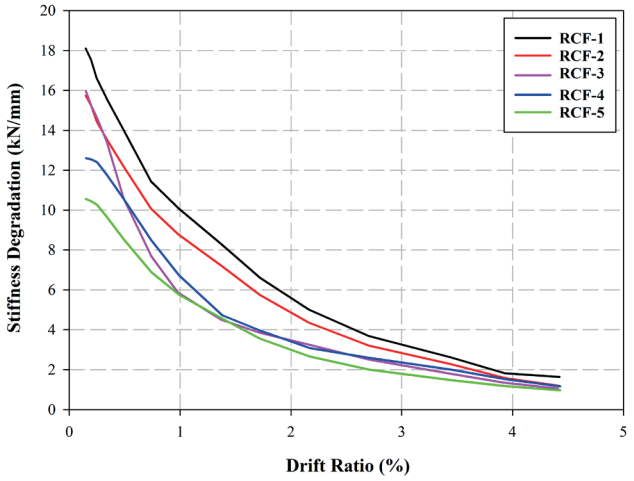


**Fig. 20** Calculation of secant stiffness for each loading cycle

When Table 5 and Fig. 21 are examined, it has been determined that the openings left in the infill walls significantly decrease the stiffness. Comparative stiffness degradation values relative to the reference specimen are given in Fig. 22 and Table 6.

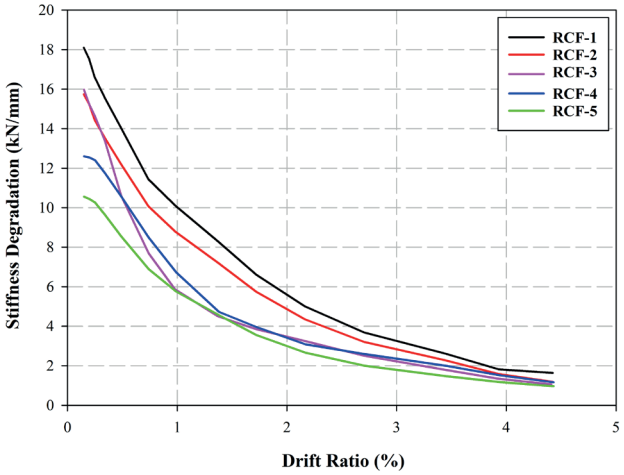


**Fig. 21** Stiffness degradation of the specimens

### 4.4 Displacement ductility

Ductility is the property of deformation or displacement beyond the elastic limit without a significant change in load carrying capacity. When determining displacement ductility ($\mu$), load-displacement backbone curves are used. In the backbone curve, the displacement corresponding to the intersection of the line drawn from the maximum load and the tangent drawn from the origin point is determined as $\Delta y$, and the final displacement corresponding to the 20% strength decrease is determined as $\Delta u$ Displacement ductility was calculated according to Fig. 23 [30]. Calculated displacement ductility is given in Table 7.

### 4.5 Failure patterns

In order to create crack maps, images of reinforced concrete frames with infill walls were recorded with high resolution cameras capable of recording 60 frames per second video during the experiment. Afterwards, the images were examined in detail and the resulting cracks and the corresponding drift ratios were determined. The crack map and failure pattern of the RCF-1 test specimen are given in Fig. 24.

When Fig. 24 is examined, a symmetrical behavior is observed in the reference specimen. At the beginning of the experiment, minor local damages and settling cracks occurred. When the 1% drift ratio is reached, diagonal cracks are formed. In the later stages of the experiment, shear cracks occurred at 2% and 3.5% drift ratios and the plaster was completely separated from the surface at certain points. When all the cycles were completed and the experiment was terminated, the wall did not collapse, and the plaster and aerated concrete blocks continued to hold at certain points.

**Table 5** Stiffness values at different steps of cycles

| Specimen code | Cycle number | Push | | | Cycle Number | Pull | | |
|---|---|---|---|---|---|---|---|---|
| | | P (kN) | Δ (mm) | Stiffness (kN/mm) | | P (kN) | Δ (mm) | Stiffness (kN/mm) |
| RCF-1 | 1 | 52.94 | 2.58 | 20.52 | 1 | 40.50 | 2.58 | 15.70 |
| | 3 | 78.96 | 4.30 | 18.36 | 3 | 63.95 | 4.30 | 14.87 |
| | 6 | 157.19 | 12.90 | 12.19 | 6 | 137.95 | 12.90 | 10.69 |
| | 9 | 206.95 | 30.10 | 6.88 | 9 | 190.41 | 30.11 | 6.32 |
| | 12 | 155.61 | 60.19 | 2.59 | 12 | 159.63 | 60.21 | 2.65 |
| | 9(max) | 206.95 | 30.10 | 6.88 | 9(max) | 190.41 | 30.11 | 6.32 |
| RCF-2 | 1 | 46.04 | 2.58 | 17.84 | 1 | 35.22 | 2.58 | 13.65 |
| | 3 | 68.66 | 4.30 | 15.97 | 3 | 55.61 | 4.30 | 12.93 |
| | 6 | 137.77 | 12.68 | 10.87 | 6 | 119.55 | 12.90 | 9.27 |
| | 9 | 179.95 | 30.10 | 5.98 | 9 | 165.57 | 30.11 | 5.50 |
| | 12 | 135.32 | 60.20 | 2.25 | 12 | 138.81 | 60.21 | 2.31 |
| | 8(max) | 183.00 | 24.07 | 7.60 | 9(max) | 165.57 | 30.11 | 5.50 |
| RCF-3 | 1 | 50.67 | 2.53 | 20.03 | 1 | 31.03 | 2.58 | 12.03 |
| | 3 | 71.69 | 4.30 | 16.67 | 3 | 54.28 | 4.31 | 12.59 |
| | 6 | 95.73 | 12.86 | 7.44 | 6 | 101.84 | 12.87 | 7.91 |
| | 9 | 104.28 | 30.00 | 3.48 | 9 | 126.74 | 30.02 | 4.22 |
| | 12 | 104.04 | 60.00 | 1.73 | 12 | 112.59 | 60.05 | 1.87 |
| | 11(max) | 116.34 | 47.15 | 2.47 | 10(max) | 130.96 | 37.74 | 3.47 |
| RCF-4 | 1 | 32.02 | 2.58 | 12.41 | 1 | 31.14 | 2.58 | 12.07 |
| | 3 | 56.53 | 4.30 | 13.15 | 3 | 51.66 | 4.31 | 11.99 |
| | 6 | 118.70 | 12.93 | 9.18 | 6 | 100.62 | 12.93 | 7.78 |
| | 9 | 131.29 | 30.16 | 4.35 | 9 | 107.80 | 30.17 | 3.57 |
| | 12 | 242.29 | 60.32 | 4.02 | 12 | 117.01 | 60.34 | 1.94 |
| | 9(max) | 131.29 | 30.16 | 4.35 | 12(max) | 117.01 | 60.34 | 1.94 |
| RCF-5 | 1 | 33.26 | 2.58 | 12.89 | 1 | 21.34 | 2.58 | 8.27 |
| | 3 | 51.44 | 4.31 | 11.94 | 3 | 37.05 | 4.31 | 8.60 |
| | 6 | 90.48 | 12.93 | 7.00 | 6 | 86.60 | 12.93 | 6.70 |
| | 9 | 101.75 | 30.16 | 3.37 | 9 | 112.57 | 30.17 | 3.73 |
| | 12 | 87.00 | 60.32 | 1.44 | 12 | 90.27 | 60.34 | 1.50 |
| | 9(max) | 101.75 | 30.16 | 3.37 | 8(max) | 118.46 | 24.14 | 4.91 |

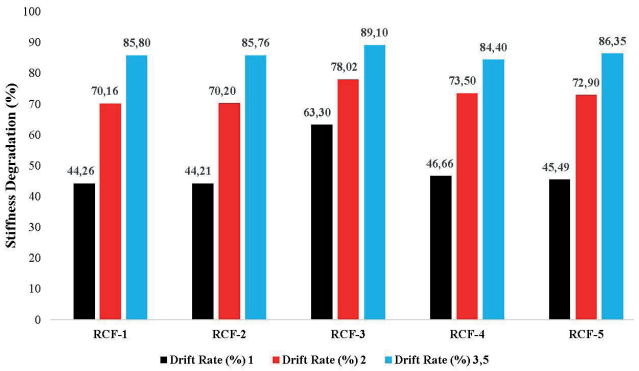


**Fig. 22** Comparative stiffness degradation

The crack map and failure pattern of the RCF-2 test specimen are given in Fig. 25.

When Fig. 25 is examined, it is seen that diagonal cracks are formed at the 1% drift ratio, starting from the column-beam and column-base connection and continuing to the corners of the window opening. In the further loading steps of the experiment, it is seen that shear cracks started to form, and, in some areas, spills occurred in the plaster (2% drift ratio and 3.5% drift ratio). After the 3.5% drift ratio, the aerated concrete blocks above the window space started to move together with the frame by forming a separate band and behaved independently from the

**Table 6** Comparative stiffness degradation values of the specimens

| Drift Rate (%) | | RCF-2 | RCF-3 | RCF-4 | RCF-5 |
|---|---|---|---|---|---|
| 0 | RCF-1 | 13.04 | 11.77 | 30.40 | 41.67 |
| 1 | RCF-1 | 13.04 | 41.96 | 33.39 | 43.03 |
| 2 | RCF-1 | 13.15 | 35.00 | 38.33 | 47.04 |
| 3.5 | RCF-1 | 12.84 | 32.30 | 23.74 | 43.97 |

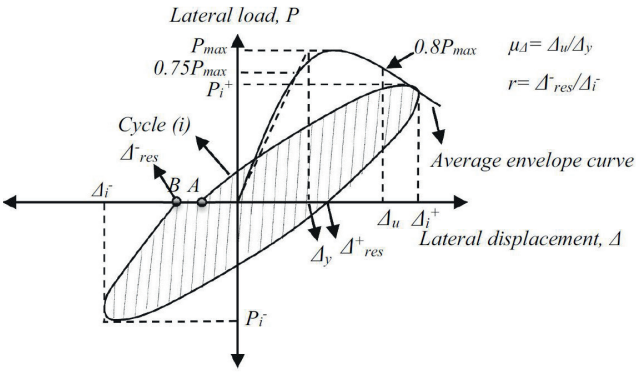


**Fig. 23** Ductility parameters of the specimens [30]

parts under it. The RCF-2 specimen continued its plane-frame behavior after this point, as the wall's contribution to energy dissipation disappeared. As a result of the experiment, plastic hinge occurred at the bottom of the column.

The crack map and failure pattern of the RCF-3 test specimen are given in Fig. 26.

When the failure pattern of the RCF-3 specimen is examined (Fig. 26), the aerated concrete blocks located between the two windows at a 1% drift ratio were damaged and completely separated from the wall. As a result, a band independent of the wall formed at the top and began to behave in the same way as the frame. Therefore, while shear cracks occurred in the wall at a 2% drift ratio, bending cracks occurred in the column at the same time and plastic hinge began at the bottom of the column. When the 3.5% drift ratio is reached, the plaster has spilled and there has been an increase in bending cracks in the columns.

The crack map and failure pattern of the RCF-4 test specimen are given in Fig. 27.

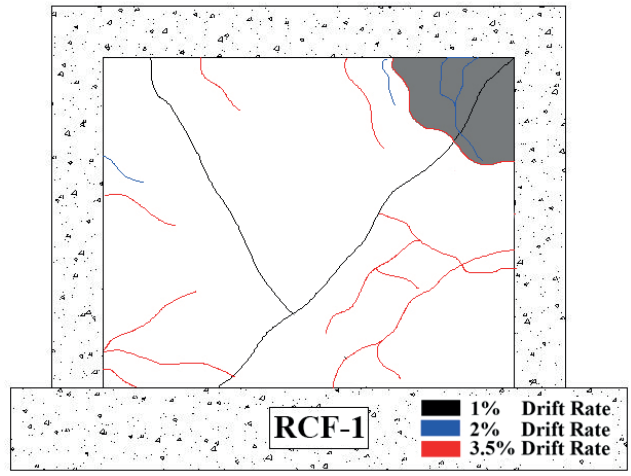


(a)

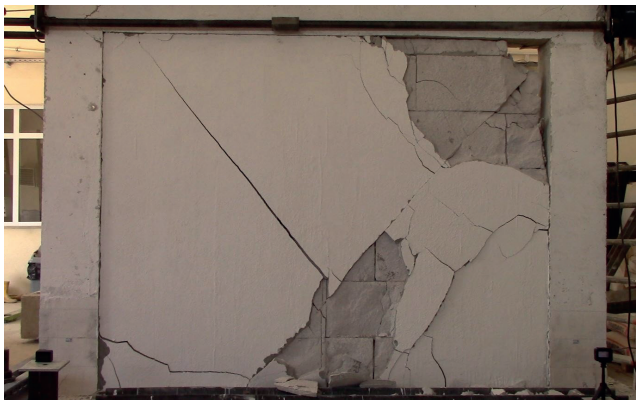

(b)

**Fig. 24** (a) Crack map, (b) Failure pattern of RCF-1

When Fig. 27 is examined, it is seen that local damages started on the door opening, which was a weak section in the first cycles, and plaster spills occurred. The part to the right of the door opening was separated from the wall at the beginning of the experiment and started to move independently with the frame. While the crack widths increased at the 2% drift ratio, plastic hinge started at the bottom of the columns. In the following cycles, the wall did not contribute to the load carrying capacity and the load carrying capacity decreased with the hinging.

**Table 7** Ductility parameters of the specimens

| Specimen Code | Failure Drift Rate (%)* | Maximum Load in Push Direction (kN) | Maximum Load in Pull Direction (kN) | Push Direction | | | Pull Direction | | |
|---|---|---|---|---|---|---|---|---|---|
| | | | | Δ*y*(mm) | Δ*u*(mm) | Δ*u*/Δ*y* | Δ*y*(mm) | Δ*u*(mm) | Δ*u*/Δ*y* |
| RCF-1 | 3.5 | 210.45 | 190.41 | 16.52 | 51.71 | 3.13 | 17.98 | 62.28 | 3.46 |
| RCF-2 | 3.5 | 183.00 | 165.57 | 16.54 | 51.02 | 3.08 | 17.65 | 62.12 | 3.52 |
| RCF-3 | 3.5 | 116.34 | 130.00 | 7.49 | 67.15 | 8.97 | 13.86 | 63.38 | 4.57 |
| RCF-4 | 3.94 | 131.28 | 117.01 | 13.91 | 67.00 | 4.82 | 10.55 | 73.98 | 7.01 |
| RCF-5 | 3.5 | 101.70 | 117.46 | 6.76 | 67.00 | 9.91 | 16.03 | 56.43 | 3.52 |

*(Drift corresponding to 0.8Fmax)

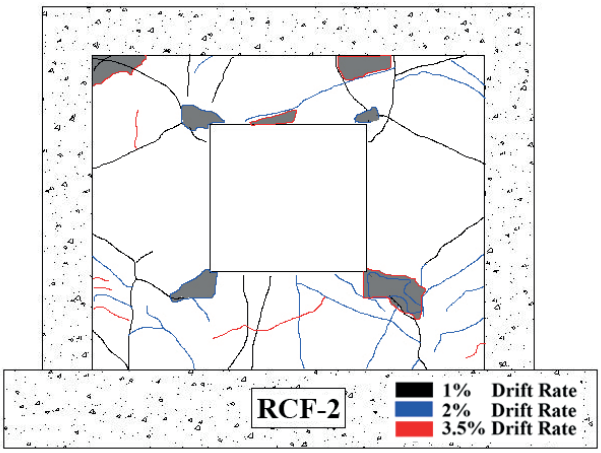


(a)

(b)

**Fig. 25** (a) Crack map, (b) Failure pattern of RCF-2

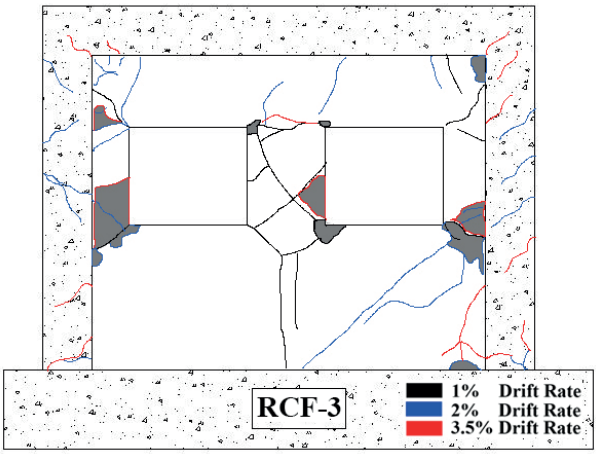


(a)

(b)

**Fig. 26** (a) Crack map, (b) Failure pattern of RCF-3

The crack map and failure pattern of the RCF-5 test specimen are given in Fig. 28.

When Fig. 28 is examined, it is seen that the block between the door and window opening in the RCF-5 frame is separated from the wall at the beginning of the experiment due to the sliding movement, as in the RCF-3 example. After this point, the band remaining on the window and door opening started to slide, moving together with the frame. As a result, bending cracks occurred in the columns at a 2% drift ratio. Hinging started at the bottom of the column and the frame continued its plane movement until the end of the experiment.

## 5 Conclusions

The main results obtained in this study, in which the behavior of RC frames with in-filled walls with different opening ratios and positions are examined, are reported below.

- It has been observed that the positions and dimensions of the openings left in the infill wall significantly alter and decrease the load carrying capacity.
- RCF-1, RCF-2, RCF-3, RCF-4, and RCF-5 samples showed the best performance in load carrying capacity, respectively.
- When the energy dissipation capacities were compared with the RCF-1, a 13%, 33.5%, 31.9% and 42.3% decrease was observed for the other specimens, respectively.
- Although the opening ratios in the RCF-2, RCF-3 and RCF-4 samples were equal, the difference in the opening locations changed their energy dissipation capacity.
- RCF-1 showed the best performance in initial stiffness and stiffness degradations, as well as in load-carrying and energy dissipation capacities.
- Location of the wall openings completely change the failure mode of the RC frame.

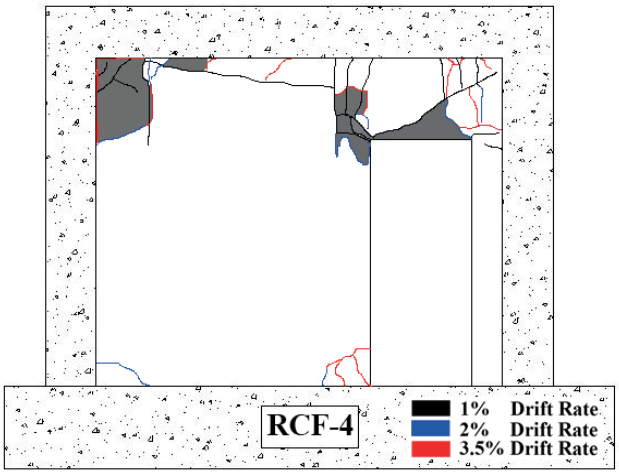


(a)

(b)

**Fig. 27** (a) Crack map, (b) Failure pattern of RCF-4

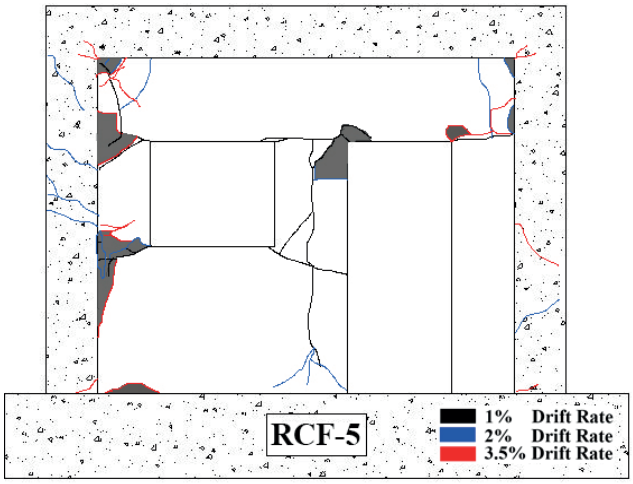


(a)

(b)

**Fig. 28** (a) Crack map, (b) Failure pattern of RCF-5

The test results show that the openings left in the infill walls significantly change the frame behavior. It has been observed that the increase in the opening ratio also decrease important parameters such as energy dissipation capacity and load carrying capacity. It has been determined that even though the opening ratios are the same, the opening positions can change the behavior. Therefore, it is suggested that infill walls, which are generally neglected in the design, should not be neglected and that the design of RC structures should be done accordingly.

## References

[1] Qian, K., Lan, D.-Q., Fu, F., Li, B. "Effects of infilled wall opening on load resisting capacity of RC frames to mitigate progressive collapse risk", Engineering Structures, 223, 111196, 2020. https://doi.org/10.1016/j.engstruct.2020.111196

[2] Eren, N., Brunesi, E., Nascimbene, R. "Influence of masonry infills on the progressive collapse resistance of reinforced concrete framed buildings", Engineering Structures, 178, pp. 375–394, 2019. https://doi.org/10.1016/j.engstruct.2018.10.056

[3] Bikçe, M., Emsen, E., Erdem, M. M., Bayrak, O. F. "An investigation on behavior of RC frames with non-interacting infill wall", Engineering Structures, 245, 112920, 2021. https://doi.org/10.1016/j.engstruct.2021.112920

[4] Axley, J. W., Bertero, V. V. "Infill panels: Their influence on seismic response of buildings", Earthquake Engineering Research Center, Berkeley, CA, USA, Rep. UCB/EERC-79/28, 1979.

[5] Smith, B. S. "Lateral stiffness of infilled frames", Journal of the Structural Division, 88(6), pp.183–199, 1962. https://doi.org/10.1061/JSDEAG.0000849

[6] Günay, M. S., Mosalam, K. M. "Structural engineering reconnaissance of the April 6, 2009, Abruzzo, Italy, earthquake, and lessons learned", University of California, Berkeley, CA, USA, Rep. 2010-105, 2010.

[7] Misir, I. S. "Potential use of locked brick infill walls to decrease soft-story formation in frame buildings", Journal of Performance of Constructed Facilities, 29(5), 04014133, 2015. https://doi.org/10.1061/(ASCE)CF.1943-5509.0000633

[8] Murty, C. V. R., Jain, S. K. "Beneficial influence of masonry infill walls on seismic performance of RC frame buildings", In: 12th World Conference on Earthquake Engineering, Auckland, New Zealand, 2000, Paper No: 1790.

[9] Campione, G., Cavaleri, L., Macaluso, G., Amato, G., Di Trapani, F. "Evaluation of infilled frames: an updated in-plane-stiffness macro-model considering the effects of vertical loads", Bulletin of Earthquake Engineering, 13(8), pp. 2265–2281, 2015. https://doi.org/10.1007/s10518-014-9714-x

[10] Di Trapani, F., Shing, P. B., Cavaleri, L. "Macroelement Model for In-Plane and Out-of-Plane Responses of Masonry Infills in Frame Structures", Journal of Structural Engineering, 144(2), 04017198, 2018. https://doi.org/10.1061/(ASCE)ST.1943-541X.0001926

[11] Furtado, A., Rodrigues, H., Arêde, A., Varum, H. "Influence of the in Plane and Out-of-Plane Masonry Infill Walls' Interaction in the Structural Response of RC Buildings", Procedia Engineering, 114, pp. 722–729, 2015. https://doi.org/10.1016/j.proeng.2015.08.016

[12] Massumi, A., Mahboubi, B., Ameri, M. R. "Seismic response of RC frame structures strengthened by reinforced masonry infill panels", Earthquake and Structures, 8(6), pp. 1435–1452, 2015. https://doi.org/10.12989/eas.2015.8.6.1435

[13] Ricci, P., Di Domenico, M., Verderame, G. M. "Empirical-based out-of-plane URM infill wall model accounting for the interaction with in-plane demand", Earthquake Engineering & Structural Dynamics, 47(3), pp. 802–827, 2018. https://doi.org/10.1002/eqe.2992

[14] Cheng, X., Zou, Z., Zhu, Z., Zhai, S., Yuan, S., Mo, Y., Chen, W., He, J. "A new construction technology suitable for frame partitioned infill walls with sliding nodes and large openings: Test results", Construction and Building Materials, 258, 119644, 2020. https://doi.org/10.1016/j.conbuildmat.2020.119644

[15] Shan, S., Li, S., Kose, M. M., Sezen, H., Wang, S. "Effect of partial infill walls on collapse behavior of reinforced concrete frames", Engineering Structures, 197, 109377, 2019. https://doi.org/10.1016/j.engstruct.2019.109377

[16] De Angelis, A., Pecce, M. R. "Out-of-plane structural identification of a masonry infill wall inside beam-column RC frames", Engineering Structures, 173, pp. 546–558, 2018. https://doi.org/10.1016/j.engstruct.2018.06.072

[17] Binici, B., Canbay, E., Aldemir, A., Demirel, I. O., Uzgan, U., Eryurtlu, Z., Bulbul, K., Yakut, A. "Seismic behavior and improvement of autoclaved aerated concrete infill walls", Engineering Structures, 193, pp. 68–81, 2019. https://doi.org/10.1016/j.engstruct.2019.05.032

[18] Buitrago, M., Bertolesi, E., Sagaseta, J., Calderón, P. A., Adam, J. M. "Robustness of RC building structures with infill masonry walls: Tests on a purpose-built structure", Engineering Structures, 226, 111384, 2021. https://doi.org/10.1016/j.engstruct.2020.111384

[19] Prakash, M., Satyanarayanan, K. S. "Experimental study on progressive collapse of reinforced concrete frames under a corner column removal scenario", Materials Today: Proceedings, 40(S1), pp. S69–S74, 2020. https://doi.org/10.1016/j.matpr.2020.03.718

[20] Jalaeefar, A., Zargar, A. "Effect of infill walls on behavior of reinforced concrete special moment frames under seismic sequences", Structures, 28, pp. 766–773, 2020. https://doi.org/10.1016/j.istruc.2020.09.029

[21] Furtado, A., Rodrigues, H., Arêde, A. "Experimental and numerical assessment of confined infill walls with openings and textile-reinforced mortar", Soil Dynamics and Earthquake Engineering, 151, 106960, 2021. https://doi.org/10.1016/j.soildyn.2021.106960

[22] Decanini, L. D., Liberatore, L., Mollaioli, F. "Strength and stiffness reduction factors for infilled frames with openings", Earthquake Engineering and Engineering Vibration, 13(3), pp. 437–454, 2014. https://doi.org/10.1007/s11803-014-0254-9

[23] Mansouri, A., Marefat, M. S., Khanmohammadi, M. "Analytical estimation of lateral resistance of low-shear strength masonry infilled reinforced concrete frames with openings", The Structural Design of Tall and Special Buildings, 27(6), e1452, 2018. https://doi.org/10.1002/tal.1452

[24] Mohammadi, M., Nikfar, F. "Strength and Stiffness of Masonry-Infilled Frames with Central Openings Based on Experimental Results", Journal of Structural Engineering, 139, pp. 974–984, 2013. https://doi.org/10.1061/(ASCE)ST.1943-541X.0000717

[25] Applied Technology Council "Interim Testing Protocols for Determining the Seismic Performance Characteristics of Structural and Nonstructural Components", Federal Emergency Management Agency, Washington, DC, USA, Rep. FEMA 461, 2007.

[26] Arslan, M. E., Celebi, E. "An experimental study on cyclic behavior of aerated concrete block masonry walls retrofitted with different methods", Construction and Building Materials, 200, pp. 226–239, 2019. https://doi.org/10.1016/j.conbuildmat.2018.12.132

[27] Arslan, M. E., Emiroğlu, M., Yalama, A. "Structural behavior of rammed earth walls under lateral cyclic loading: A comparative experimental study", Construction and Building Materials, 133, pp. 433–442, 2017. https://doi.org/10.1016/j.conbuildmat.2016.12.093

[28] Park, R. "Evaluation of ductility of structures and structural assemblages from laboratory testing", Bulletin of the New Zealand Society for Earthquake Engineering, 22(3), pp. 155–166, 1989. https://doi.org/10.5459/bnzsee.22.3.155-166

[29] Xue, W., Yang, X. "Seismic tests of precast concrete, moment-resisting frames and connections", PCI Journal, 55(3), pp. 102–121, 2010. https://doi.org/10.15554/pcij.06012010.102.121

[30] Demir, U., Unal, G., Goksu, C., Saribas, I., Ilki, A. "Post-fire Seismic Behavior of RC Columns Built with Sustainable Concrete", Journal of Earthquake Engineering, 26(13), pp. 6869–6892, 2021. https://doi.org/10.1080/13632469.2021.1927897